Eur Biophys J (2007) 36:787–793
DOI 10.1007/s00249-007-0157-z

ORIGINAL PAPER

Modulation of the reaction cycle of the Na^+:Ca^{2+}, K^+ exchanger

Natascia Vedovato · Giorgio Rispoli

Received: 30 December 2006 / Revised: 2 March 2007 / Accepted: 15 March 2007 / Published online: 6 April 2007

Abstract Ca^{2+} concentration in retinal photoreceptor rod outer segment (OS) strongly affects the generator potential kinetics and the receptor light adaptation. The response to intense light stimuli delivered in the dark produce potential changes exceeding 40 mV: since the Ca^{2+} extrusion in the OS is entirely controlled by the Na^+:Ca^{2+}, K^+ exchanger, it is important to assess how the exchanger ion transport rate is affected by the voltage and, in general, by intracellular factors. It is indeed known that the cardiac Na^+:Ca^{2+} exchanger is regulated by Mg-ATP via a still unknown metabolic pathway. In the present work, the Na^+:Ca^{2+}, K^+ exchanger regulation was investigated in isolated OS, recorded in whole-cell configuration, using ionic conditions that activated maximally the exchanger in both forward and reverse mode. In all species examined (amphibia: *Rana esculenta* and *Ambystoma mexicanum*; reptilia: *Gecko gecko*), the forward (reverse) exchange current increased about linearly for negative (positive) voltages and exhibited outward (inward) rectification for positive (negative) voltages. Since hyperpolarisation increases Ca^{2+} extrusion rate, the recovery of the dark level of Ca^{2+} (and, in turn, of the generator potential) after intense light stimuli results accelerated. Mg-ATP increased the size of forward and reverse exchange current by a factor of ∼2.3 and ∼2.6, respectively, without modifying their voltage dependence. This indicates that Mg-ATP regulates the number of active exchanger sites and/or the exchanger turnover number, although via an unknown mechanism.

Keywords Ion exchanger · Ion transporter · Retina · ATP · Rod photoreceptor

Abbreviations

OS	photoreceptor rod outer segment
V_h	holding potential
I–V	Current to voltage characteristics

Introduction

The vertebrate photoreceptor exchanger (Yau and Nakatani 1984; Hodgkin et al. 1987) plays a crucial role in phototransduction, since the sustained exchanger activity in light induces intracellular Ca^{2+} fall, which in turn triggers several mechanisms taking part in dark state recovery and light adaptation of the photoreceptor (reviewed in Rispoli 1998; Moriondo and Rispoli 2003). It has been found that the exchanger imports four Na^+ ions (forward mode of exchange) for every Ca^{2+} and K^+ ion extruded (Cervetto et al. 1989; Schnetkamp et al. 1989; Rispoli et al. 1995), thereby accounting for one net positive charge imported per exchange cycle. The rod photoreceptor exchanger (NCKX1) is the first member of the new gene family *SLCA24*, comprising at least four other members having broad expression pattern: for instance, the retinal cone

Proceedings of the XVIII Congress of the Italian Society of Pure and Applied Biophysics (SIBPA), Palermo, Sicily, September 2006.

N. Vedovato · G. Rispoli (✉)
CNISM, Dipartimento di Biologia ed Evoluzione,
Sezione di Fisiologia e Biofisica and Centro di Neuroscienze,
Università di Ferrara, via Borsari 46,
44100 Ferrara, Italy
e-mail: rsg@unife.it

Present Address:
N. Vedovato
Laboratory of Cardiac/Membrane Physiology,
The Rockefeller University, 1230 York Avenue,
New York, NY 10021, USA

exchanger NCKX2 has been found in brain and in retinal ganglion cells as well (reviewed in Schnetkamp 2004).

The peculiar architecture of the rod outer segment (OS), in which the entire transduction machinery, the cGMP channels and the exchanger are segregated, makes the patch-clamp recording from mechanically isolated OS a powerful technique to study photoreceptor physiology. OS dialysed with nucleotides supports normal phototransduction, showing that the manipulations employed to isolate the OS preserves the integrity of the entire transduction machinery (Rispoli et al. 1993) and, consequently, of the exchanger as well. Under bright light, the exchanger is the only OS current source, therefore this current can be recorded under whole-cell, voltage-clamp conditions without using any ion channel blocker, that could aspecifically interfere with the exchanger operation (Rispoli et al. 1995).

Intense light stimuli delivered in the dark produce changes in the generator potential exceeding 40 mV: since the exchanger is the sole Ca^{2+} extrusion mechanism present in the OS plasma membrane, it is important to assess its voltage dependency. Moreover, intracellular factors may affect the exchanger operation and/or its voltage sensitivity as well: for instance, it is now well established that the cardiac Na^+:Ca^{2+} exchanger is regulated by ATP (as originally shown by Hilgemann and Ball 1996), although the metabolic pathway related to its action is still unknown (DiPolo et al. 2004). In the present work, the modulation by voltage and ATP of the Na^+:Ca^{2+},K^+ exchanger was investigated by recording the exchanger current in whole-cell configuration from OS isolated from amphibia and reptilia, to assess also any difference related to species diversity.

Methods

Animals and preparation

Ambystoma mexicanum larvae and *Rana esculenta* frogs were kept in filtered, running tap water in small tanks at room temperature (20–23°C); *Tokay gecko* lizards were kept in transparent boxes endowed with small cardboard dens, rocks and wood sticks, kept to a constant temperature (30°C) and humidity (80%). All animals were fed two–three times a week with honey worms and maintained in a natural light–dark cycle. Animal experiments and care were performed in compliance with the Declaration of Helsinki guidelines and approved by a local ethical committee.

Before dissection, the animals were dark adapted (≈4 h), anaesthetised with ether (*Tokay gecko*) or by immersion in a tricaine methane sulphonate solution (1 g/l in water; *Rana esculenta* and *Ambystoma mexicanum*) and then decapitated. Both eyes were removed from the head and hemisected. The back half of the eyeball was cut into four pieces that were stored in oxygenated Ringer solution on ice and used when needed. The retina was "peeled" from an eyecup piece and was gently triturated in ~5 µl of Ringer, using a fire-polished Pasteur pipette or fine forceps to obtain the isolated OS. All these manipulations were made in the dark using infrared illumination and an infrared viewer (Find-R-Scope, FJW Optical Systems, Palatine, IL, USA).

Solutions

Cells were bathed in Ringer's solution having the following composition (in mM): 115 NaCl, 3 KCl, 10 HEPES free acid (*N*-[2-hydroxyethyl]piperazine-*N*′-[2-ethanesulfonic acid]), 0.6 $MgCl_2$, 0.6 $MgSO_4$, 1.5 $CaCl_2$, 10 glucose for amphibia, and 160 NaCl, 3.3 KCl, 1 $CaCl_2$, 1.7 $MgSO_4$, 10 HEPES and 10 glucose for reptilia. The perfusion and the patch pipette solutions (specified in the text and figure legends) were designed to activate maximally the exchanger in both the forward and reverse mode. The nucleotide modulation of the exchanger was assessed by adding 5 or 10 mM of adenosine 5′-triphosphate, dipotassium salt, or adenosine 5′-triphosphate, magnesium salt to the internal solutions. 0 Ca^{2+} external solutions contained 5 mM EGTA free acid (ethylene glycol-bis-(β-aminoethyl ether) *N*,*N*,*N*′,*N*′,-tetraacetic acid); 0 Ca^{2+} internal solutions contained 0.01 or 12 mM BAPTA (1,2-bis(*O*-aminophenoxy)ethane-*N*,*N*,*N*′,*N*′-tetraacetic acid) tetrapotassium salt. Osmolality of all internal, bath and perfusion solutions was checked with a micro-osmometer (Hermann Roebling, Messtechnik, Berlin, Germany) and was ≈260 mOsm/kg for amphibia and ≈320 mOsm/kg for reptilia. All solutions were buffered to pH ≈7.6 (amphibia) and to pH ≈7.4 (reptilia) with 10 mM HEPES and NaOH, KOH or LiOH depending upon whether the solution contained high Na^+, high K^+ or 0 Na^+, respectively. All chemicals were purchased from Sigma Chemical Co. (St. Louis, MO, USA).

Patch-clamp recordings and data analysis

In room lights, a fluid drop (500 µl) of the triturated retina was transferred to the recording chamber on the microscope stage (TE 300, Nikon, Tokyo, Japan), fitted with an Eppendorf micromanipulator (model 5171, Eppendorf, Hamburg, Germany). OS were illuminated with an ultrabright infrared LED (900 nm) and viewed on a TV monitor connected to a contrast enhancement camera (Till Photonics, Planegg, Germany) coupled to the microscope.

Electrical recordings were carried out using the patch-clamp recording technique in the "whole-cell" configuration under visual control at room temperature (20–22°C). Pipettes were pulled in the conventional manner from 50 µl glass capillaries (Drummond, Broomall, PA, USA), and fire-polished to a pipette resistance of ≈5 MΩ. Recordings

were obtained employing an Axopatch 200B amplifier (Molecular Devices, Sunnyvale, CA, USA) and were filtered at 2 kHz via an eight-pole Butterworth filter (VBF/8 Kemo, Beckenham, UK). Current was sampled on-line at 10 kHz by a Digidata 1322A connected to the SCSI port of a Pentium computer running the pClamp software package (version 9.0; Molecular Devices), and stored on disk. Seal resistance (4.7 ± 0.5 GΩ, $n = 78$), access resistance (30 ± 2 MΩ, $n = 78$), membrane resistance (1.2 ± 0.1 GΩ, $n = 78$) and cell capacitance (*Ambystoma mexicanum*: 29.3 ± 1.0 pF, $n = 23$; *Rana esculenta*: 11.3 ± 1.6 pF; $n = 25$; *Tokay gecko*: 46.8 ± 3.6 pF, $n = 30$) were determined using repetitive −10 mV voltage pulses; the holding potential (V_h) was 0 or −20 mV. The current to voltage relationships (*I–V*s) were obtained using 100 ms voltage pulses, from −80 to +80 mV in 20 mV step, intervalled by 100 ms steps to V_h.

The external solution was changed rapidly (typically in ∼50 ms) by moving horizontally with a computer controlled stepping motor a multibarrelled perfusion pipette placed in front of the recorded OS (developed in collaboration with De Angelis s.r.l., Genova, Italy). The solutions flowing in the perfusion pipette were fed by means of precision syringes (Hamilton, Reno, NV, USA) whose piston was moved by a computer-controlled motor (typical perfusion speed: 15 µl/min). The perfusion solution was removed by a peristaltic pump (OEM 400VDL/VM3, Watson Marlow, Wilmington, MA, USA).

Data were low-pass filtered off-line at 200 Hz using a Gaussian filter to obtain the *I–V*s; tracings shown in Figs. 1a, b, 3a, 4a, b, and 5a and b were instead filtered at 25 Hz to cancel the current spikes generated by the −10 mV pulses, delivered to measure the seal and access resistance, and the cell capacitance. Data analysis was performed using Clampfit (included in the pClamp package); figures and statistics were prepared using SigmaPlot (version 8.0; Jandel Scientific, San Rafael, CA, USA), results are given as mean ± SEM.

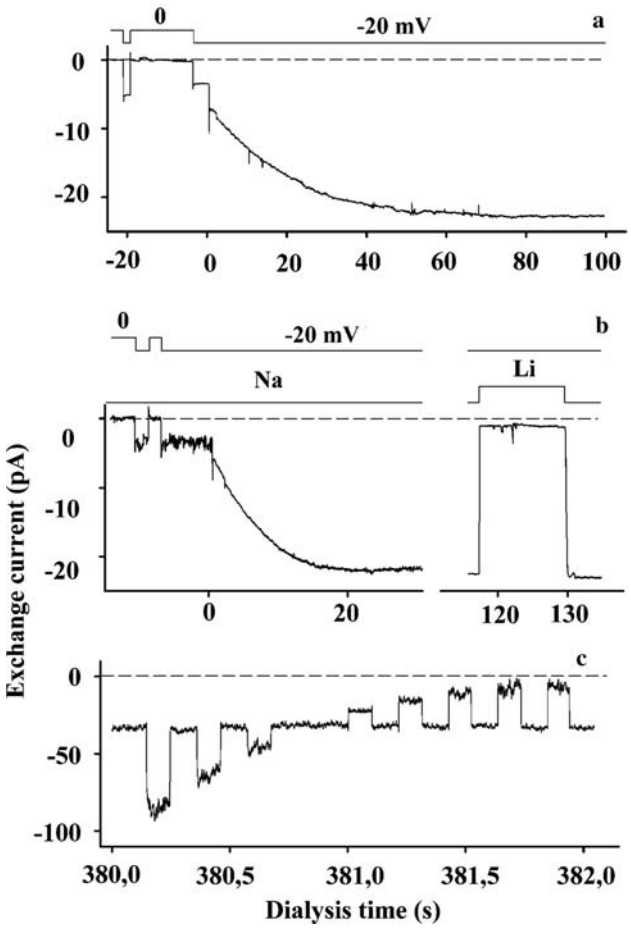

Fig. 1 Steady state forward exchange current. **a**, **b** Typical recordings obtained upon dialysing an isolated rod outer segment (OS) of *Rana esculenta* (**a**) and of *Ambystoma mexicanum* larvae (**b**) with 20 mM Ca^{2+} + 95 mM K^+ and bathed in amphibia's Ringer; exchanger blockade in (**b**) was obtained upon substituting 115 mM Na^+ of Ringer's solution with 115 mM Li^+. Breakthrough to whole-cell recordings occur at 0 time; $V_h = 20$ mV. **c** Typical experiment to construct the *I–V*s shown in Fig. 2, exemplified for a *Tokay gecko* OS dialysed with 20 mM Ca^{2+} + 136 mM K^+ and bathed in reptilia's Ringer; voltage protocol as described in Methods. Average currents: -29 ± 3 pA, $n = 25$ *Tokay gecko* OS; -18 ± 4 pA, $n = 12$ *Rana esculenta* OS; -25 ± 1 pA, $n = 6$ *Ambystoma mexicanum* larvae OS; -25 ± 2 pA, $n = 43$ OS of all species averaged

Results and discussion

In the absence of Mg-ATP in the patch pipette solution, forward exchange current of stable amplitude of −25 pA ($V_h = -20$ mV) was recorded from isolated OS of all species examined, dialysed with 20 mM Ca^{2+} + > 100 mM K^+ (to maximise the current: these concentrations should be saturating for the exchanger intracellular binding sites for Ca^{2+} and K^+) and bathed in Ringer (containing 1 mM Ca^{2+}; Fig. 1). In these recordings, membrane resistance was tipically >1 GΩ and current fell to 0 as soon as external Na^+ was replaced with an equiosmolar concentration of another monovalent cation (as Li^+, Cs^+, Rb^+ or K^+; Fig. 1b), confirming the lack of any other current source but the exchanger, and the absolute requirement of external Na^+ for exchanger operation. The current to voltage (*I–V*) relationship was evaluated by subtracting the current recorded in the presence of external Na^+, in response to brief voltage pulses (as exemplified in Fig. 1c), from the current elicited by the same voltage pulses in a solution containing 0 external Na^+ (i.e. once the exchanger was blocked). The resulting *I–V*s were approximately linear for negative voltages and asymptotically approached the zero current for positive voltages (Fig. 2a), remarkably superimposing in all species examined, once normalised for the current amplitude at −80 mV (Fig. 2b).

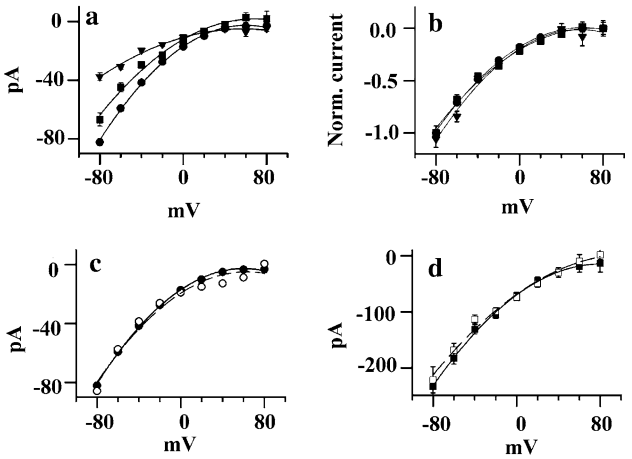

Fig. 2 Average *I–V*s of forward exchange mode at the steady state in the absence of ATP. **a** Average difference *I–V*s recorded in external Na^+ and in 0 Na^+ for *Ambystoma mexicanum* larvae (circles, $n = 15$), *Rana esculenta* (triangles, $n = 14$), and *Tokay gecko* (squares, $n = 9$). **b** The *I–V*s of (**a**) are normalised for the current amplitude at −80 mV; the current level at +80 mV was set to 0. **c**, **d** Comparison between the average leak corrected *I–V*s (*empty symbols* and *broken lines*; leak measured using ±5 mV voltage pulses during exchanger blockade in 0 external Na^+) and the average difference *I–V*s recorded in external Na^+ and in 0 Na^+ (*filled symbols* and *continuous lines*) exemplified for *Ambystoma mexicanum* larvae OS ($n = 18$) in 1 mM external Ca^{2+} (**a**) and for *Tokay gecko* OS ($n = 4$) in 0 external Ca^{2+} (**d**). Error bars in (**c**) were smaller than the symbols and were therefore not shown. *Continuous lines* in all panels are second-order polynomial interpolations to the data points

Therefore, the different shape of the IVs of Fig. 2a very likely arose from the different number of exchange sites, that may vary among the various species depending upon the OS total membrane area and the density of exchange sites. It can be therefore concluded that the exchanger voltage sensitivity is basically the same for all species examined, in the presence of ion concentrations that maximised the exchange current amplitude. As a control, the *I–V*s recorded in external Na^+ were also corrected for the leak resistance, measured using ±5 mV voltage pulses delivered once the exchanger was blocked after removing external Na^+. The resulting *I–V*s were, as expected, very similar to the one evaluated with the above subtraction method, as exemplified in Fig. 2c for an *Ambystoma mexicanum* larvae OS. All the results shown in this paper were remarkably similar for all species examined, therefore representative data is illustrated in the following using one species or another indifferently.

The exchanger turnover number is rate limited by the Ca^{2+} transport translocation kinetics (Rispoli et al. 1996): indeed, the removal of external 1 mM Ca^{2+} doubled the steady state amplitude of forward exchanger current. The removal of external Ca^{2+} did not however affect the *I–V* waveform (Fig. 2d; data collected and illustrated as in panel c) for any voltage and for all species examined, indicating that Ca^{2+} transport does not significantly affect the voltage sensitivity of the overall transport process.

In order to assess whether the exchange process was symmetrical, the OS was bathed in a solution containing Ca^{2+} and K^+ only, and dialysed with Ringer. The current amplitude recorded under these conditions was much smaller than the one recorded in forward mode. The current did not increase significantly by maximising the gradients of Na^+ and Ca^{2+} (by dialysing the OS with >100 mM Na^++12 mM BAPTA solution) and by imposing $V_h = 0$: the average current for all species examined was still ∼fivefold smaller than the average forward exchange current (Fig. 3a). This indicates that Ca^{2+} imported via reverse exchange accumulates in the cytosol, resulting in exchanger inhibition. This is expected, since Ca^{2+} is imported through the entire cell surface, its intracellular diffusion is hindered by the disk stack, and its removal relies entirely on the trade of Ca^{2+} and BAPTA between the patch pipette and cytosol through a tiny hole. In any case, exchange current was detected only if Ca^{2+} and K^+ were present on the same membrane side, and Na^+ was simultaneously present on the opposite side. Any other ionic combination different than this one gave flat *I–V*s (within ±1.5 pA) for any voltage from −80 to +80 mV once the current was corrected for the membrane resistance (measured at $V_h = 0$ mV using ±5 mV voltage pulses; Fig. 3b). This demonstrates that it was not possible to force the exchanger to work electrogenically in modes different (as, for instance, the Na^+:Ca^{2+} one) than the "normal" one (Na^+ translocated in one direction for Ca^{2+} and K^+ translocated in the opposite direction) for any voltage (even out of the physiological range). This feature has been found for the cardiac exchanger (Kang and Hilgemann, 2004) but not for other

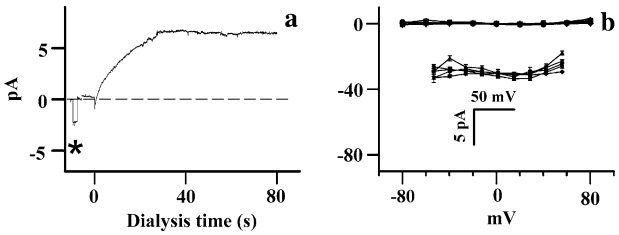

Fig. 3 Electrogenic modes of exchanger different than the forward one. **a** Largest reverse exchange current ever recorded in an *Ambystoma mexicanum* larvae OS recorded in the presence of 85 mM Na^+ + 12 mM BAPTA in the patch pipette solution, bathed in 20 mM Ca^{2+} + 95 mM K^+; $V_h = 0$ mV. Average currents: +6.3 ± 1.1 pA, $n = 21$ *Tokay gecko* OS; +3.2 ± 0.5 pA, $n = 21$ *Rana esculenta* OS; +7.4 ± 1.5 pA, $n = 5$ *Ambystoma mexicanum* larvae OS; +5.1 ± 0.6 pA, $n = 47$ OS of all species pooled. **b** Leak corrected *I–V*s in various ionic conditions, enlarged in the inset; data from the three species were pooled since they were virtually identical. The current was about 0 within ±1.5 pA from −80 to +80 mV when Na^+ was present without Ca^{2+} ($n = 6$) or without K^+ ($n = 12$), and vice versa ($n = 12$), or when Na^+, Ca^{2+} and K^+ were present on one membrane side but not on the other side ($n = 6$)

Ca^{2+} transporters, as the red blood cells Na^+:Ca^{2+} exchanger (Milanick and Frame 1991) and as the sarcoplasmic Ca^{2+} ATP-ase pump (Inesi and de Meis 1988). The strict stoichiometry of Ca^{2+} transport by the Na^+:Ca^{2+},K^+ exchanger is particularly important for vision, since uncontrolled Ca^{2+} entry by means of "channel-like" or "slippage" activity would deeply affect the photoresponse kinetics and light adaptation (Moriondo and Rispoli 2003).

In order to detect reverse exchange current circumventing the intracellular Ca^{2+} accumulation, the following protocol was employed. The OS dialysed with Na^+ only and 0 Ca^{2+} was switched from an extracellular solution containing Na^+ only and 0 Ca^{2+}, to a solution containing Ca^{2+}+K^+, using the fast perfusion system described in the "Methods". A reverse exchange current was activated, with a kinetics comparable to the solution change timing (~50 ms), upon switching the OS to the Ca^{2+}+K^+ solution. During Ca^{2+}+K^+ perfusion, current decayed exponentially due to cytosol accumulation of Ca^{2+} via reverse exchange (recordings were similar to the one shown in Figs. 4, 5). Indeed, this decay was little affected by raising the pipette K^+ from 0 to 80 mM (data not shown) but was strongly slowed down by elevating the concentration of intracellular Ca^{2+} buffer (Fig. 4a). The K^+ and Ca^{2+} accumulated during reverse exchange operation were able to promote forward exchange upon returning the OS to a solution containing Na^++EGTA. However, K^+ diffuses much faster than Ca^{2+} in the cytosol, since the disk stack is a natural Ca^{2+} buffer, therefore K^+ accumulated to a smaller extent in the cytosol than Ca^{2+}, being washed out by the patch pipette more readily than Ca^{2+}. Therefore, Ca^{2+} that had accumulated during reverse operation sufficed to activate maximal forward exchange upon returning to Na^+, but the residual K^+ concentration was too small to produce currents as large as those showed in Fig. 1. The addition of at least 20 mM K^+ to the high Na^+ dialysis solution was indeed enough to activate maximal forward exchange current and to allow the complete depletion of Ca^{2+} accumulated during the reverse exchange operation (Figs. 4b, 5a, b). As expected, the ratio between the charge imported during reverse exchange operation (150 ± 20 pC, $n = 28$) and the charge extruded during forward operation (120 ± 10 pC, $n = 28$) was ≥1 (1.4 ± 0.2, $n = 28$; some of the imported Ca^{2+} may be washed away by the pipette as a free ion or complexed with BAPTA). Since negative (positive) voltages would hasten (hamper) forward exchange and hamper (hasten) reverse exchange, V_h was set to 0 mV in all these experiments. Reverse exchange *I–V* could be determined only at the peak current attained during Ca^{2+}+K^+ perfusion, because the current decayed to a plateau level too small to have a precise estimate of the *I–V*. Therefore, 12 mM BAPTA was added to the pipette solution in order to have a peak current (indicated with *A* in Fig. 4b) lasting enough to allow the acquisition of the *I–V*.

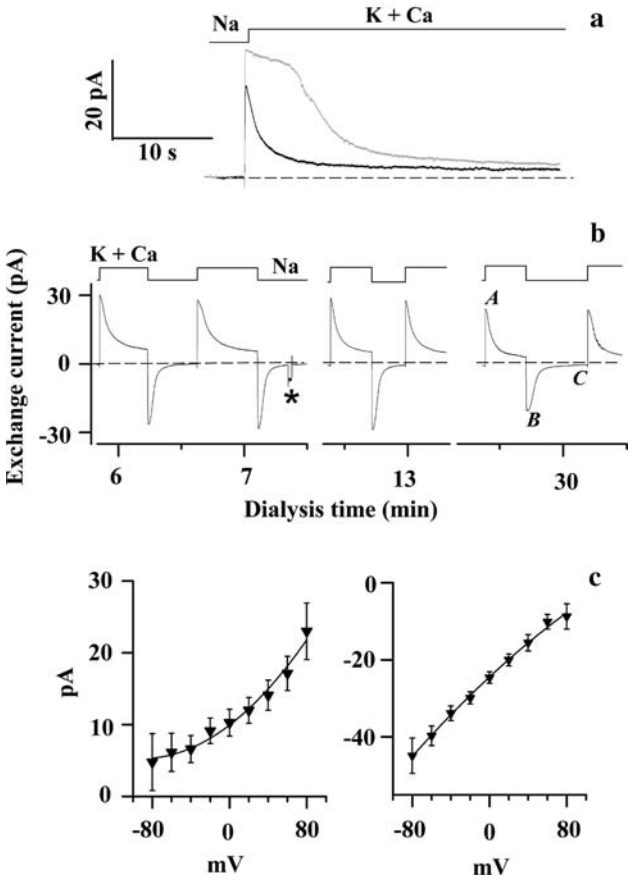

Fig. 4 Forward and reverse exchange activation in the absence of ATP. **a** Effect of BAPTA on reverse exchange, exemplified for two *Tokay gecko* OS switched from external 166 mM Na^+ + 5 mM EGTA to 20 mM Ca^{2+} + 136 mM K^+ and dialysed with 105 mM Na^+ + 60 mM K^+ + 0.01 mM BAPTA (black trace) or with 100 mM Na^+ + 20 mM K^+ + 12 mM BAPTA (total K^+: 68 mM; grey trace). **b** Recording of reverse exchange current peaks (as in *A*) exemplified in a *Rana esculenta* OS dialysed with 80 mM Na^+ + 12 mM BAPTA (total K^+: 48 mM) and switched from external 120 mM Na^+ + 5 EGTA to 20 mM Ca^{2+} + 100 mM K^+. The Ca^{2+} imported during reverse exchange suffice to activate maximal forward exchange (as in *B*) upon returning to the Na^+ solution; once the Ca^{2+} load was fully extruded, exchange current felled to 0 (*C*). Note the progressive decay of reverse (*A*) and forward (*B*) exchange current peak amplitude to a steady state level (*C*) with the dialysis time; the asterisk indicate a current jump elicited by a −20 mV pulse to check the input resistance; $V_h = 0$ mV. In (**c**), the difference *I–V* recorded *A* and in *C* (left panel), and difference *I–V* recorded in *B* and *C* (right panel), gave the steady state reverse and forward exchange *I–V*, respectively; data from three *Rana esculenta* OS averaged

The Ca^{2+} accumulated in the cytosol during reverse exchange operation allowed activation of maximal forward exchange, once returning the OS to external Na^+, lasting long enough to acquire an *I–V* (indicated with *B* in Fig. 4b). The forward and reverse exchanger *I–V*s were estimated by subtracting the *I–V* obtained respectively in *A* and *B* with the *I–V* obtained when the exchanger was inhibited (indicated with *C* in Fig. 4b), i.e. after the Ca^{2+} imported

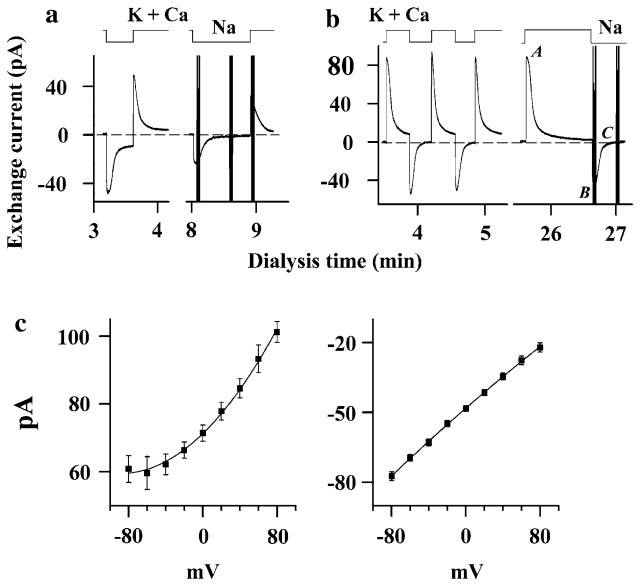

Fig. 5 Mg-ATP dependence of forward and reverse exchange. Data exemplified for a *Tokay gecko* OS; Vh = 0 mV. **a**, **b** Two OS were switched back and forth from external 166 mM Na^+ + 5 mM EGTA to 20 mM Ca^{2+} + 136 mM K^+ and dialysed with 100 mM Na^+ + 10 mM K^+ + 12 mM BAPTA and (**a**) 5 mM ATP + 0 Mg^{2+} or (**b**) 5 mM Mg-ATP. **c** Reverse (*left panel*) and forward (*right panel*) exchange *I–V* were obtained as described in Fig. 4; the vertical black bars crossing the recordings in (a) and (b) are the current spikes in response to the voltage pulses delivered to construct the *I–V*s

during reverse exchange was fully extruded by forward exchange operation. Forward and reverse exchanger *I–V*s were similar: they were approximately linear for voltages far from 0 mV and exhibited inward and outward rectification, respectively, (Fig. 4c). This indicates that the voltage sensitivity of the overall exchanger process was substantially symmetrical, at least for concentrations of the transported ions much larger than the affinity of the corresponding ion binding sites of the exchanger. However, the peak current amplitude of reverse exchange was larger than the forward one (by an average factor of 1.2 ± 0.1, $n = 39$; data from the three species were pooled), indicating that, unexpectedly, the exchanger of all species examined transported ions in the reverse mode more efficiently than in the forward (physiological) mode. One possibility is that the Ca^{2+} imported during reverse exchange operation might not be enough to fully saturate the Ca^{2+} binding sites, resulting in a reduced current amplitude once forward mode was activated in external Na^+. However, this was not the case, since the current peak amplitude was maintained for a few seconds, showing that the exchanger was working at its maximal rate during this period.

Occasionally, large forward and reverse exchange current peaks were recorded just after the breakthrough to whole-cell, that progressively decayed to a reduced amplitude that was maintained afterwards (Fig. 4b). To keep track of these time-dependent changes of exchange current amplitude, the abscissa of all figures reports the dialysis time (i.e. the time elapsed starting from the breakthrough to whole-cell recording). This result suggests the presence of an exchanger activator that was progressively washed away by the patch pipette during the recording: the most obvious component is Mg-ATP (that was lacking in all patch pipette solutions in the experiments presented so far), since Mg-ATP has been found to boost the cardiac exchanger (Hilgemann and Ball 1996). The progressive decay of exchanger current peaks was still present in the recordings from OS dialysed with 5 mM of ATP (Fig. 5a). The OS dialysis with 5 mM of Mg-ATP prevented instead this decay and the amplitude of forward and reverse exchange current peaks remained stable to the elevated amplitude or even increased throughout the recording (Fig. 5b). The forward and the reverse exchange current peaks were respectively 2.3 ± 0.4 and 2.6 ± 0.4 ($n = 21$; data pooled from the three species) larger than the corresponding peaks recorded in the absence of ATP, further confirming the unexpected more efficient ion transport in the reverse mode in respect to the physiological (forward) mode. This feature, not used under any physiological conditions in vision, is probably important in other cellular system as the cardiomyocytes, where reverse exchange occurs during normal muscle operation, contributing to the cardiac contraction (Lines et al. 2006). The dialysis with 10 mM Mg-ATP did not further increase the peak amplitudes in respect to 5 mM Mg-ATP, showing that the affinity for ATP of the exchanger regulatory site was smaller than 5 mM and that 3 mM of Mg^{2+} (i.e. the calculated free Mg^{2+} concentration in the presence of 12 mM BAPTA and 5 mM of total Mg^{2+}) sufficed to fully activate the modulatory pathway. Forward and reverse exchanger *I–V*s in the presence of Mg-ATP (Fig. 5c) were similar to the ones recorded in 0 ATP (Fig. 4c). The *I–V*s recorded in *A* or *B* was also corrected for the leak estimated in *C*: again, the resulting *I–V*s were similar to the ones shown in Fig. 5c (data not shown). It is concluded that Mg-ATP stimulates forward and reverse exchange in the same manner without affecting the shape of their *I–V*s. This indicates that Mg-ATP regulates the number of active exchanger sites and/or the exchanger turnover number, although, as for the cardiac exchanger, the mechanism of this regulation is still unknown.

All the characteristics of ion transport operated by the Na^+:Ca^{2+},K^+ exchanger from amphibia to reptilia resulted basically similar. In particular, when operating in forward mode, the exchanger appeared to behave electrically as a constant conductance for voltages in the physiological range. The exchanger Ca^{2+} extrusion rate increased of about two-fold for a voltage jump elicited by a saturating light turned on in the dark (producing a ~40 mV voltage jump in the membrane potential). This voltage-dependent

increase of Ca^{2+} extrusion rate would accelerate the fall of intracellular Ca^{2+} concentration, caused by the light-induced closure of the cGMP channels, in respect to a voltage-independent exchanger. This voltage regulation of the exchanger is therefore designed to boost the Ca^{2+}-dependent enzymes (as the guanylate cyclase and recoverin; reviewed in Moriondo and Rispoli 2003) contributing to the mechanism of light adaptation and recovery of the dark level of the generator potential once the light stimulation is ceased.

Acknowledgments This work was supported by grants from the Ministero per l'Università e la Ricerca Scientifica e Tecnologica (MURST), Roma, from CNISM "progetti innesco 2006" (project MRP), and from the "Comitato dei sostenitori dell'Università di Ferrara" (Project "Trasporto di carica fotoindotto in materiali funzionali").

References

Cervetto L, Lagnado L, Perry RJ, Robinson DW, McNaughton PA (1989) Extrusion of calcium from rod outer segments is driven by both sodium and potassium gradients. Nature 337:740–743

DiPolo R, Berberián G, Beaugè L (2004) Phosphoarginine regulation of the squid nerve Na^+/Ca^{2+} exchanger: metabolic pathway and exchanger–ligand interactions different from those seen with ATP. J Physiol 554:387–401

Hilgemann DW, Ball R (1996) Regulation of cardiac Na^+, Ca^{2+} exchange and KATP potassium channels by PIP2. Science 273:956–960

Hodgkin AL, McNaughton PA, Nunn BJ (1987) Measurement of sodium–calcium exchange in salamander rods. J Physiol 391:347–370

Inesi G, de Meis L (1988) Regulation of steady state filling in sarcoplasmic reticulum. J Biol Chem 264:5929–5936

Kang TM, Hilgemann DW (2004) Multiple transport modes of the cardiac Na^+/Ca^{2+} exchanger. Nature 427:544–548

Lines GT, Sande JB, Louch WE, Mork HK, Grottum P, Sejersted OM (2006) Contribution of the Na^+/Ca^{2+} exchanger to rapid Ca^{2+} release in cardiomyocytes. Biophys J 91(3):779–792

Milanick MA, Frame MD (1991) Kinetic models of Na–Ca exchange in ferret red blood cells interaction of intracellular Na, extracellular Ca, Cd, and Mn. Ann N Y Acad Sci 639:604–615

Moriondo A, Rispoli G (2003) A step-by-step model of phototransduction cascade shows that Ca^{2+} regulation of guanylate cyclase accounts only for short-term changes of photoresponse. Photochem Photobiol Sci 2(12):1292–1298

Rispoli G (1998) Calcium regulation of phototransduction in vertebrate rod outer segments. J Photochem Photobiol B 44(1):1–20

Rispoli G, Navangione A, Vellani V (1995) Transport of K^+ by Na^+–Ca^{2+}, K^+ exchanger in isolated rods of lizard retina. Biophys J 69:74–83

Rispoli G, Navangione A, Vellani V (1996) Turnover rate and number of Na^+–Ca^{2+},K^+ exchange sites in retinal photoreceptors. Ann N Y Acad of Sci 779:346–356

Rispoli G, Sather WA, Detwiler PB (1993) Visual transduction in dialyzed detached rod outer segments from lizard retina. J Physiol 465:513–537

Schnetkamp PP, Basu DK, Szerencsei RT (1989) Na^+–Ca^{2+} exchange in bovine rod outer segments requires and transports K^+. Am J Physiol 257:153–157

Schnetkamp PP (2004) The SLC24 Na^+/Ca^{2+}–K^+ exchanger family: vision and beyond. Pflugers Arch 447:683–688

Yau KW, Nakatani K (1984) Electrogenic Na–Ca exchange in retinal rod outer segment. Nature 311:661–663